



Effect of a self-rotating oxygen lance system on mass transfer between slag and molten steel

Qi Gao¹ · Wei Wu¹ · Jian-guo Zhi^{2,3} · Bo Zhang¹ · Xiang-chen Li¹

Received: 14 December 2019 / Revised: 13 June 2020 / Accepted: 14 June 2020 / Published online: 24 November 2020
© China Iron and Steel Research Institute Group 2020

Abstract

To improve the efficiency of the steelmaking process, a system of self-rotating lance was designed, and corresponding cold simulation mechanism was developed. The influence of the self-rotating lance on the mass transfer rate between slag and molten steel was investigated by comparing this novel system with the traditional oxygen lance. The results show that the self-rotating lance can stably rotate with a gas jet as the power source. The mass transfer rate increases with an increase in the top and bottom blow flow rates and with a decline in the lance position. Approximately 13.7% of the top blow flow rate is converted to stirring energy, which is approximately twice that of the traditional oxygen lance, and the mass transfer rate can increase by over 30%. Furthermore, the impact energy can be concentrated at different depths of the molten bath by adjusting the rotational speed. With the same energy density, the mass transfer rate produced by the self-rotating lance is higher; however, the influence of the energy density on the mass transfer rate is low when the rotational speed is 30–50 r/min.

Keywords Self-rotating lance · Reaction force · Rotational speed · Mass transfer rate · Impact energy

1 Introduction

As steel companies have become increasingly eager to reduce production costs, medium- or high-phosphorus iron ore is now used in the ironmaking process [1, 2]. However, the smelting process of the medium- or high-phosphorus hot metal has several problems, such as a long dephosphorization time, large slag volumes, and slag splashing. Lemitar Steel [3, 4] and Tata Steel [5] use high-phosphorus hot metal to produce low-phosphorus steel, which is a process that is difficult to control because excess slag is produced. In Japan, high-phosphorus low-silicon hot metal is smelted by blowing oxygen through the bottom of the

converter. This approach can be used for hot metal with a phosphorus content of about 0.14%. However, this process is not suitable for hot metal with a higher phosphorus content [6]. In European countries, the top blow-spray lime powder approach is used to treat medium- and high-phosphorus hot metal [7]. Two different methods can be used for reducing the amount of slag produced during steelmaking: the top-blown basic oxygen converter method and the top lance powder-spraying oxygen converter method [8, 9]. In these methods, the dephosphorization efficiency is effectively improved by expanding the slag–molten steel interface and increasing the stirring efficiency of the molten bath. However, the equipment and processes are sophisticated that is a challenge to promote.

The oxygen lance plays a vital role in decarburizing, dephosphorizing, slag melting, etc. [10, 11]. The fluid flow characteristics of the traditional top-blown oxygen lance have been investigated and analyzed [12]. Wang et al. [13] studied the flow field of the 4-hole oxygen lance jet with numerical simulation. Li et al. [14] studied three oxygen lance jets with cold model experiment and numerical simulation. They found that the effective impact area of the four-hole oxygen lance is significantly higher than that of the five-hole oxygen lance. Lv and Zhu [15] designed a

✉ Wei Wu
wuweineu@163.com

¹ Metallurgical Technology Research Department, Central Iron and Steel Research Institute, Beijing 100081, China

² Inner Mongolia Enterprise Key Laboratory of Rare Earth Steel Products Research and Development, Baotou 014010, Inner Mongolia, China

³ Inner Mongolia Baotou Steel Union Co., Ltd., Baotou 014010, Inner Mongolia, China

coherent jet oxygen lance for steelmaking experiment and found that the end-point phosphorus content dropped from 0.024% to 0.016%. The swirl-type oxygen lance can improve stirring effect on molten bath because it can generate not only axial and radial forces, but also tangential force [16]. The swirl-type oxygen lance has been previously applied in a vanadium extraction converter [17] and a 120-t dephosphorization converter [18] to improve the dynamic conditions of the molten bath. Liu et al. [19] designed a new type of oxygen lance to enhance the mass transfer between slag and molten steel in the steelmaking process. When the dynamic oxygen lance is used, the impact area of the jet increases significantly as the nozzle continuously moves. This improves the dynamic conditions of the steelmaking process [20]. Díaz et al. [21] found that the rotating lance produces smaller bubbles in comparison with the fixed lance, which has a slower floating speed and a higher mass transfer rate between gas and liquid. Souza Costa et al. [22] investigated the desulfurization of hot metal and found that the rate of desulfurization and dephosphorization improved by 20% and 30%, respectively, when a rotating lance is used, in comparison with a fixed lance. Fan and Zeng [23] deemed that the free spray lance accelerates the melting of the lime and reduces the splashing of the hot metal.

In this study, a self-rotating lance system and the corresponding cold model were designed. Furthermore, the influence of the dynamic oxygen lance on the mass transfer between the slag and molten steel was studied, which provides a reference for the application of the dynamic oxygen lance.

2 Experimental equipment and methods

2.1 Self-rotating oxygen lance design

The self-rotating lance, which is connected to the air supply system via a rotational joint, is fixed on the support platform using a fixing device and a thrust bearing. At the end of the lance, there are four flow-shaped connecting pipes, which rotate in a circumferential direction according to the angle α , connecting the four single-hole Laval nozzles. The system is shown in Fig. 1. When blowing, the lance is subjected to the reaction force of the jet. Because of the angle α , the reaction force has a tangential component centered on the main shaft of the lance, which acts as the motive force. The distance between the blow direction and the main shaft of the lance acts as the power arm. Those make up a rotational torque acting on the lance. When the rotational torque is higher than the resistive

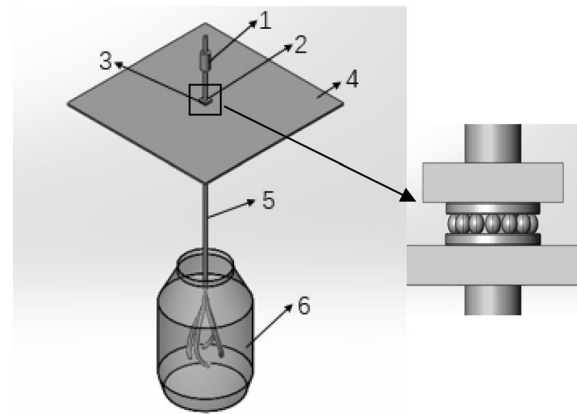


Fig. 1 Schematic representation of converter with self-rotating oxygen lance mechanism. 1 Rotational joint; 2 fixing device; 3 thrust bearing; 4 support platform; 5 oxygen lance; 6 converter

torque generated by the thrust bearing and the rotational joint, the lance can rotate freely without any external force.

2.2 Experimental parameters and methods

A cold model of a 120-t converter, built with a ratio of 1:6 from organic glass, and the self-rotating lance cold simulation system were designed. To ensure dynamic similarity between the model and the prototype, the modified Froude number Fr' was selected as a similarity number, which is commonly used in the cold simulation experiment of the converter [24, 25]. From the calculation, when the top blow intensity of the converter is 3.92, 4.04, and 4.20 $\text{m}^3 \text{t}^{-1} \text{min}^{-1}$, the blow flow rate of the corresponding model is 131, 135, and 140 $\text{m}^3 \text{h}^{-1}$, respectively.

Experiments were conducted using the self-rotating lance system, where an infrared non-contact tachometer measured the rotational speed. The oxygen lance could rotate at 30–50 r/min when the arm and α were 130 mm and 25°, respectively, and the top blow flow rate was 131 $\text{m}^3 \text{h}^{-1}$. By adjusting the pressure between the fixing device and the thrust bearing, the lance could rotate at 30–50 or 70–90 r/min with a flow rate of 135 $\text{m}^3 \text{h}^{-1}$, and rotate at 70–90 or 110–130 r/min with a flow rate of 140 $\text{m}^3 \text{h}^{-1}$.

Mass transfer experiments were also conducted, where water, oil, and benzoic acid were used to simulate the molten steel, slag, and the mass transfer element, respectively. Before the experiment, 0.033 mol L^{-1} of benzoic acid was dissolved in the oil. At the beginning of the test, 75 L of water was added to the converter, and after 3 min of a stable blow, 3 L of the oil–benzoic acid mixture was added to the molten bath. To reduce the amount of deviation, the bucket containing the oil–benzoic acid solution

was placed in a position that was 500 mm from the liquid level in the converter and then poured into the center of the molten bath within 2 s. The pH value of water was measured in real time using a pH meter and recorded automatically every 15 s. Further, a camera was used to record the change of the molten bath. The experimental parameters were set according to the converter production data, as given in Table 1.

2.3 Relationship between pH value and benzoic acid concentration in water

The relationship between the concentration of the benzoic acid dissolved in water and the pH level was obtained in the preliminary experiment, as shown in Fig. 2. According to the relationship, the concentration of benzoic acid in water can be calculated using the pH value of water.

2.4 Calculating mass transfer coefficient of solute at slag–molten steel interface

Metallurgical processes occur at extremely high temperatures, which increases the interface chemical reaction rate. Thus, the resistance of the mass transfer process of the

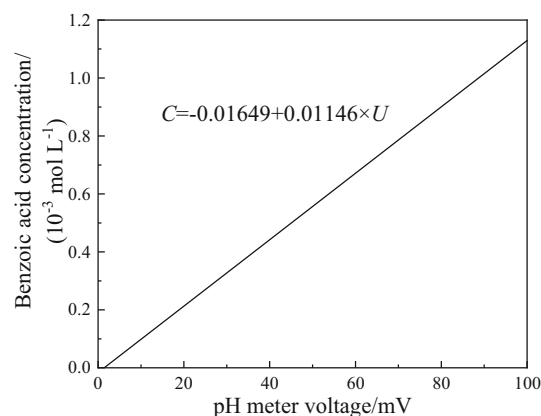


Fig. 2 Relationship between benzoic acid concentration in water and pH meter voltage. C Concentration of benzoic acid dissolved in water; U pH meter voltage

reactants and products in the molten steel and slag is the reaction rate-limiting links. The relationship of the solute content between the slag and steel:

$$J = k_m A (C_m C_m^i) = k_s A (C_s^i - C_s) \quad (1)$$

where J is the diffusion flux of the solute; k_m is the solute mass transfer coefficient of the molten steel; k_s is the mass

Table 1 Parameters of mass transfer water simulation experiment

No.	Oxygen lance type	Top blow flow rate/(m ³ h ⁻¹)	Rotational speed/(r min ⁻¹)	Lance position/mm	Bottom blow flow rate/(m ³ h ⁻¹)
1	Self-rotating	131	0	233	0
2	Self-rotating	131	0	283	0
3	Self-rotating	131	0	333	0
4	Self-rotating	131	30–50	233	0
5	Self-rotating	131	30–50	283	0
6	Self-rotating	131	30–50	333	0
7	Self-rotating	135	0	283	0
8	Self-rotating	135	30–50	283	0
9	Self-rotating	135	70–90	283	0
10	Self-rotating	140	0	283	0
11	Self-rotating	140	70–90	283	0
12	Self-rotating	140	110–130	283	0
13	Self-rotating	131	30–50	283	1.2
14	Self-rotating	131	30–50	283	1.8
15	Self-rotating	131	30–50	283	2.4
16	Traditional	131		283	0
17	Traditional	135		283	0
18	Traditional	140		283	0
19	Traditional	131		233	0
20	Traditional	131		333	0
21	Traditional	131		283	1.2
22	Traditional	131		283	1.8
23	Traditional	131		283	2.4

transfer coefficient of the solute reactants in the slag; C_m and C_m^i are the concentrations of the solute in the molten steel and the solution interface film, respectively; C_s^i and C_s are the concentrations of the solute reaction products in the slag and slag interface film, respectively; and A is the area of the slag–molten steel interface.

Equation (2) can be obtained as [26]:

$$\ln \left[1 - \left(h + \frac{V_m}{V_s} \right) \frac{C_m}{C_{s,0}} \right] = -kA \cdot t \quad (2)$$

$$\frac{1}{V_m} + \frac{1}{hV_s}$$

where $C_{s,0}$ is the initial concentration of benzoic acid in engine oil; V_m and V_s are the volume of water and engine oil, respectively; h is the equilibrium distribution ratio of solute in slag–molten steel; k is the total mass transfer coefficient of the solute from the molten steel to slag; and t is the time.

It is difficult to measure the contact area between the oil and water during the blowing process. However, the product of the mass transfer coefficient and the boundary area can be obtained by Eq. (2). Therefore, kA can be used to express the mass transfer rate.

3 Experimental results and analysis

3.1 Mass transfer velocity

During the experiment, it was found that the pH of the water solution, after having decreased rapidly, began gradually decelerating at the beginning of the blowing process. After approximately 8 min of blowing, the pH returned to the equilibrium value with an ultimate distribution ratio of 8. Using Eq. (2), the benzoic acid mass transfer rate in the oil–water mixture can be calculated as shown in Table 2.

From Table 2, the influence of the blowing parameters on the mass transfer rate can be obtained, as shown in Fig. 3.

Figure 3 shows that when either the self-rotating lance or the traditional oxygen lance is used, the mass transfer rate increases with an increase in the top and bottom blow flow rates and a decline in the lance position. When the self-rotating lance is used, the mass transfer rate obviously increases, where the influence of the bottom blow flow rate on the mass transfer rate is 7.2 times that of the top blow flow rate. Moreover, for the case of the traditional lance, it is 13.8 times. Kohtani [27] reports that most of the energy

Table 2 Mass transfer rate of benzoic acid in oil–water mixture under different blow conditions

No.	Oxygen lance type	Top blow flow rate/ (m ³ h ⁻¹)	Rotational speed/ (r min ⁻¹)	Lance position/ mm	Bottom blow flow rate/ (m ³ h ⁻¹)	kA / (cm ³ s ⁻¹)
1	Self-rotating	131	0	233	0	727.1
2	Self-rotating	131	0	283	0	651.2
3	Self-rotating	131	0	333	0	575.2
4	Self-rotating	131	30–50	233	0	783.5
5	Self-rotating	131	30–50	283	0	720.9
6	Self-rotating	131	30–50	333	0	695.0
7	Self-rotating	135	0	283	0	712.2
8	Self-rotating	135	30–50	283	0	821.2
9	Self-rotating	135	70–90	283	0	789.3
10	Self-rotating	140	0	283	0	757.5
11	Self-rotating	140	70–90	283	0	832.2
12	Self-rotating	140	110–130	283	0	638.7
13	Self-rotating	131	30–50	283	1.2	818.3
14	Self-rotating	131	30–50	283	1.8	861.4
15	Self-rotating	131	30–50	283	2.4	929.3
16	Traditional	131	–	283	0	578.5
17	Traditional	135	–	283	0	604.3
18	Traditional	140	–	283	0	635.7
19	Traditional	131	–	233	0	618.3
20	Traditional	131	–	333	0	481.8
21	Traditional	131	–	283	1.2	725.4
22	Traditional	131	–	283	1.8	759.9
23	Traditional	131	–	283	2.4	787.5

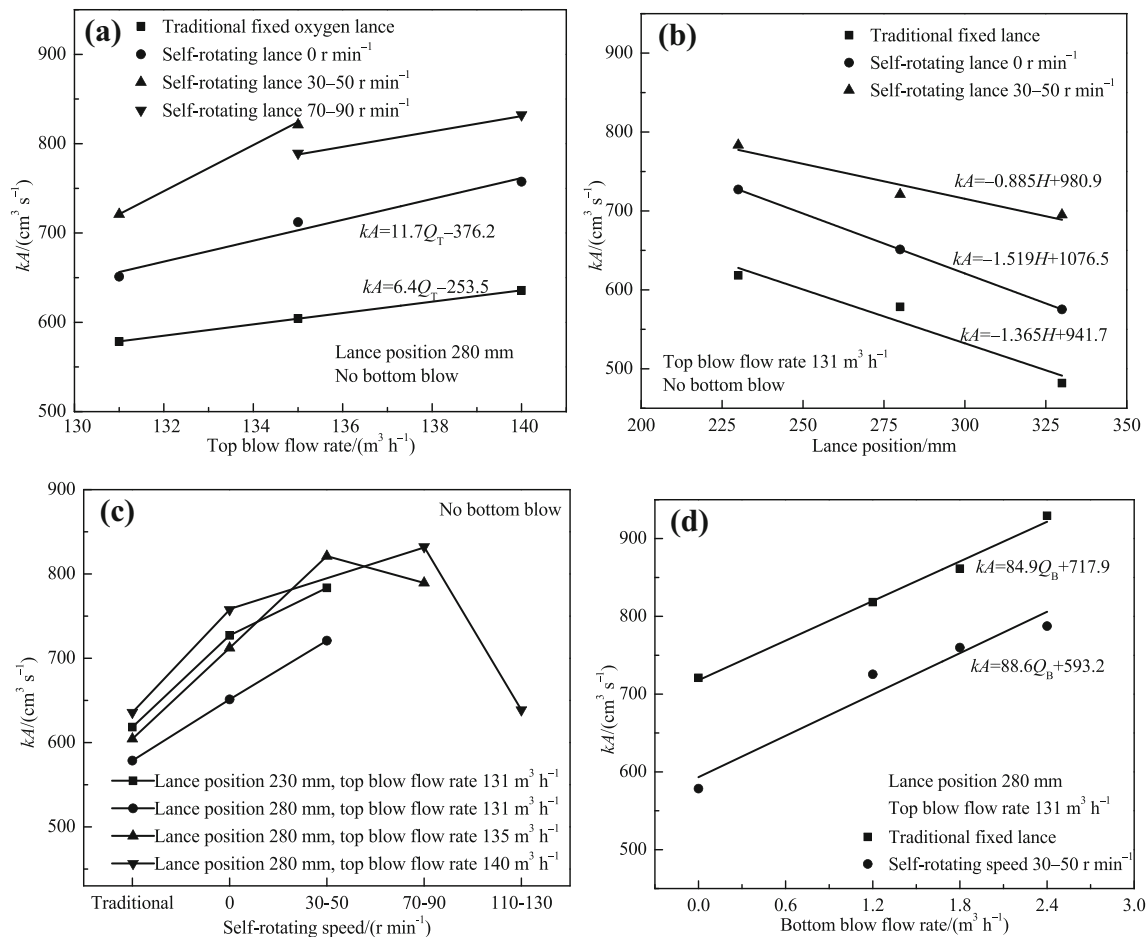


Fig. 3 Effect of top blow flow rate Q_T (a), lance position H (b), self-rotating speed (c), and bottom blow flow rate Q_B (d) on mass transfer rate

generated by the top blow gas is consumed on the impact surface, and only 6%–10% is converted into sufficient stirring power, while most of the bottom blow gas can be converted into agitation power. If the bottom blow energy is entirely converted into stirring energy, it can be concluded that 13.8% of the top blow flow is converted into stirring energy for the self-rotating lance, which is about twice that of the traditional oxygen lance.

Figure 3c shows that when the rotational speed is 0, 30–50, 70–90, and 110–130 r/min, the mass transfer rate increases by 16.8%, 30.1%, 29.1%, and 4.7%, respectively. With increased rotational speed, the mass transfer rate initially increases and then decreases. As the rotational speed rises to 110–130 r/min, the mass transfer rate reduces to a value close to that of the traditional oxygen lance. The main reason for this is that the jet disperses and the molten bath rotates owing to the impact of the jet, thereby resulting in the increase in the relative motion between the oil and water. When turning at 30–50 r/min, the jet impact energy acts on a large ring in the molten bath and the area of jet impact increases. Moreover, the direction of the lance rotation is opposite to that of the fluid flow, and thus, the

impact of the jet on the fixed position of the molten bath has a specific interval. Consequently, the oil on the surface of the molten bath accumulates near the wall of the furnace and then moves along the wall to the bottom of the molten bath, which increases the mass transfer rate. As the rotational speed continues to increase, the impact depth decreases, and the impact energy is excessively concentrated on the surface of the molten bath. When this happens, the residence time of the oil droplets in water would be reduced, causing a decline in the mass transfer rate.

3.2 Molten bath emulsification according to different blow parameters

After the blowing process with the self-rotating lance or traditional oxygen lance comes the emulsification of the molten baths, as shown in Figs. 4 and 5.

The gas jet forces the oil droplets into the molten bath, causing the oil and water to fuse, which reduces the transmittance of the molten bath. The molten bath emulsification can be evaluated considering the degree of light transmission and the shaded area in the molten bath.

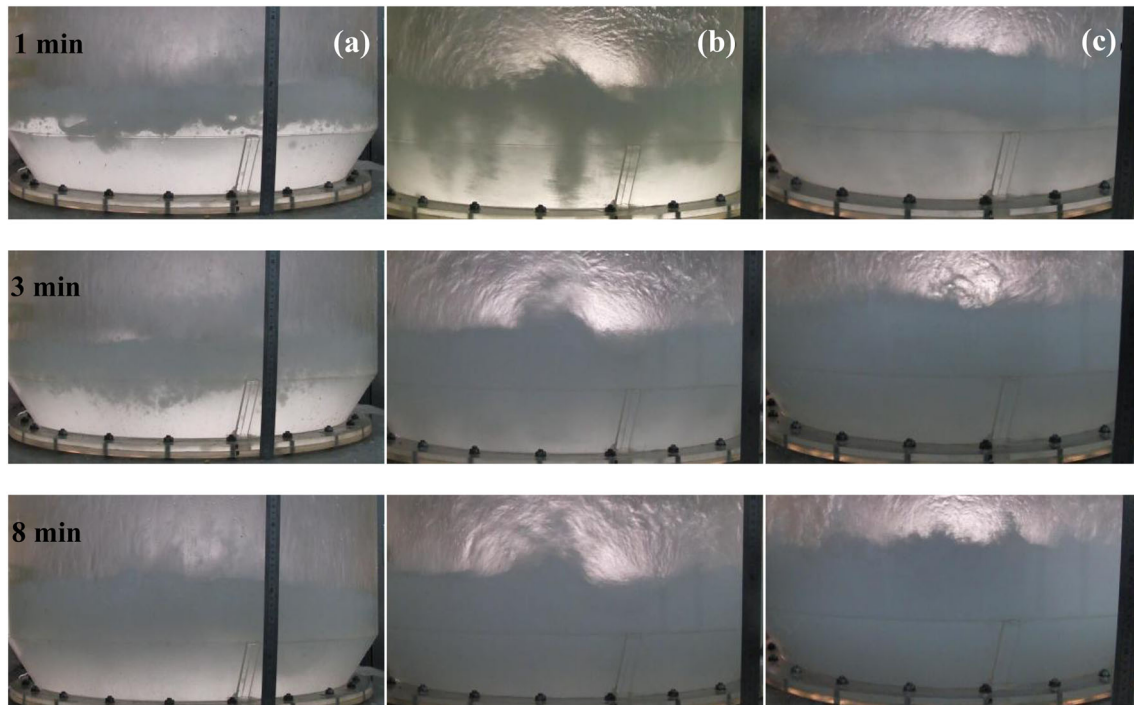


Fig. 4 Molten bath emulsification conditions at different time with top blow flow rate of $131 \text{ m}^3 \text{ h}^{-1}$ and lance position of 280 mm for traditional lance (a), self-rotating lance at 0 r min^{-1} (b), and self-rotating lance at $30\text{--}50 \text{ r min}^{-1}$ (c)

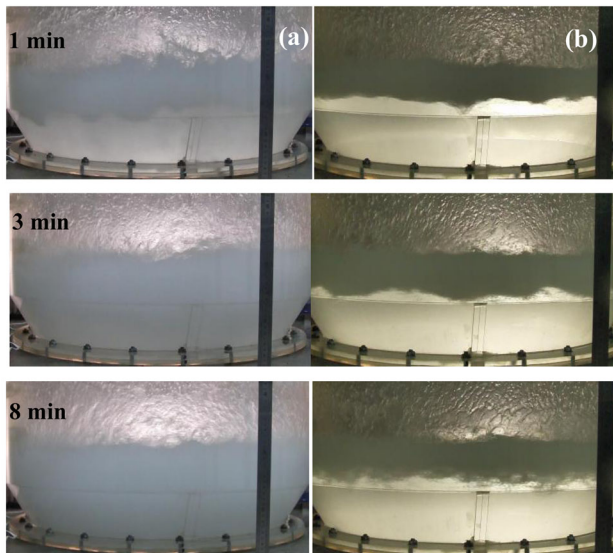


Fig. 5 Molten bath emulsification at different time for self-rotating lance with a lance position of 280 mm for top blow flow rate of $135 \text{ m}^3 \text{ h}^{-1}$ at $70\text{--}90 \text{ r min}^{-1}$ (a) and top blow flow rate of $140 \text{ m}^3 \text{ h}^{-1}$ at $110\text{--}130 \text{ r min}^{-1}$ (b)

Figures 4 and 5 show that the emulsification speed of the molten bath varied significantly according to the different blow conditions. For instance, when the traditional oxygen lance was used, the oil gradually diffused to the middle of the molten bath after 3 min, and after 8 min, the emulsification process was almost complete. When the self-

rotating lance was used, the emulsification speed improved significantly, especially when the rotational speed was approximately $30\text{--}50 \text{ r/min}$, and emulsification was finished after 3 min of blowing. As the rotational speed improved to $70\text{--}90 \text{ r/min}$, the emulsification speed slightly declined. Even at $110\text{--}130 \text{ r/min}$, the emulsification rate of the molten bath was still low after 8 min of blowing, and the middle and bottom sections of the molten bath were free of emulsification. This can be attributed to the fact that the impact area increases significantly when the self-rotating lance is used, which makes the fluid in the molten bath flow uniformly, and the oil and water relative flow increases. However, when the rotational speed increases, the impact depth reduces, which makes the stirring energy concentrate toward the surface of the molten bath, thereby reducing the emulsification speed of the molten bath.

4 Discussion

The agitation effect of the gas jet on the molten bath depends on three factors: top blow flow rate, bottom blow flow rate, and lance position. The stirring energy density could be used for linking these factors to establish a relationship with the mass transfer characteristics of the molten bath. The stirring energy density equations are outlined below [28].

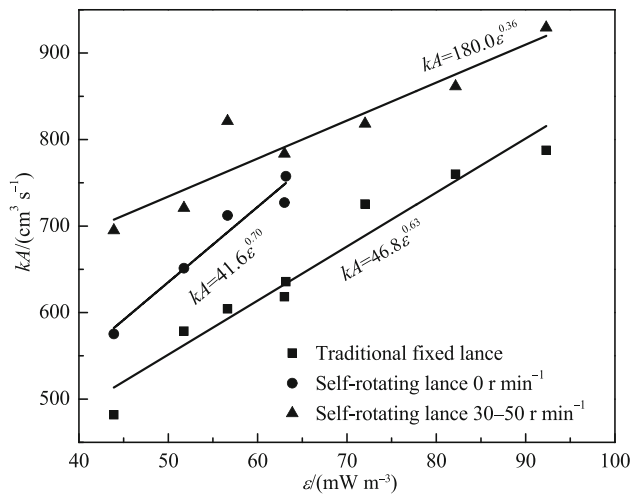


Fig. 6 Relationship between energy density and mass transfer rate

$$\varepsilon_T = 1.83 \times 10^{-5} \frac{Q_T^3}{d^2 HV_1} \quad (3)$$

$$\varepsilon_B = 14.25 \frac{Q_B}{V_1} T_1 \left(1 + \frac{L}{1.47} \right) \quad (4)$$

$$\varepsilon = \varepsilon_B + 0.1\varepsilon_T \quad (5)$$

where ε_T is the top blow stirring energy density; ε_B is the bottom blow stirring energy density; ε is the total stirring energy density; d is the throat diameter of the oxygen lance; V_1 is the volume of the fluid in the molten bath; L is the depth of the molten bath; and T_1 is the temperature of the solution.

The relationship between stirring energy density and mass transfer rate is shown in Fig. 6.

Figure 6 shows that the energy density has a linear relationship with the mass transfer rate. In comparison with the traditional lance, the mass transfer rate is higher for the self-rotating lance with the same energy density, and the energy density has a more significant influence on the mass transfer rate at 0 r/min but has a lower impact at 30–50 r/min. This is because the jet polymerization of the traditional oxygen lance partially counteracts the energy and reduces the effective utilization of the jet. For the self-rotating lance, the nozzles separate from each other, which makes the jet stream disperse, resulting in the maximum use of kinetic energy. However, when the rotational speed is 30–50 r/min, the area of impact is large and the homogenization of the molten bath flow field is high, which is difficult to increase with an increased energy density. Therefore, the mass transfer rate increases mainly because of the retention time of oil droplets in water [29]. When the rotational speed is very high, the impact energy is concentrated on the upper section of the molten bath, where

most of the oil droplets enter, which reduces the retention time of the oil droplets in water.

5 Conclusions

1. The mass transfer rate increases with an increase in the top and bottom blow flow rates and a decline in the lance position.
2. Approximately 13.8% of the top blow flow rate is converted into stirring energy, which is about twice that of the traditional lance. When the rotational speed is 0, 30–50, 70–90, or 110–130 r/min, the mass transfer rate increases by 16.8%, 30.1%, 29.1%, and 4.7%, respectively.
3. The impact energy can be concentrated at different depths of the molten bath by adjusting the rotational speed. Similarly, the molten bath emulsification speed and the mass transfer speed can be adjusted.
4. The mass transfer rate is higher and increases as the energy density increases; however, the influence of the energy density on the mass transfer speed is low when the rotational speed is 30–50 r/min.

Acknowledgements This research was financed by the National Key Research and Development Program with Project Number 2017YFB0304000 and the Beijing Natural Science Foundation with Project Number 2172057 in China.

References

- [1] V. Hernandez, K. Peake, A. Dalvi, R. Brown, J. Olurin, T. O'Farrell, M. Zhou, B. Liu, I. Cameron, in: R.E. Ashburn, K.D. Hickey, C.P. Brown, K.J. McGhee (Eds.), AISTech Proceedings, Association for Iron and Steel Technology, Pittsburgh, PA, USA, 2013, pp. 519–526.
- [2] H.R. Kokal, M.P. Singh, V.A. Naydyonov, in: C. Young, A. Alfantazi, C. Anderson, A. James, D. Dreisinger, B. Harris (Eds.), Electrometallurgy and Environmental Hydrometallurgy, Vol. 2, The Minerals, Metals and Materials Society, Vancouver, BC, Canada, 2003, pp. 1517–1530.
- [3] T. Mukherjee, A. Chatterjee, Bull. Mater. Sci. 19 (1996) 893–903.
- [4] B. Deo, J. Halder, B. Snoeijer, A. Overbosch, R. Boom, Ironmak. Steelmak. 32 (2005) 54–60.
- [5] S.K. Choudhary, S.N. Lenka, A. Ghosh, Ironmak. Steelmak. 34 (2007) 343–349.
- [6] S. Basu, A.K. Lahiri, S. Seetharaman, ISIJ Int. 47 (2007) 766–768.
- [7] B. Trantini, P. Vayssiere, J. Iron Steel Inst. 6 (1959) 143.
- [8] A. Clerc, J. Dufflot, A. Constant, Rev. Met. Paris 61 (1964) 545–567.
- [9] W.Y. Yang, Y. Gan, M.L. Wang, China Metallurgy 21 (2011) No. 3, 4–10.
- [10] Y. Doh, P. Chapelle, A. Jardy, G. Djambazov, K. Pericleous, G. Ghazal, P. Gardin, Metall. Mater. Trans. B 44 (2013) 653–670.
- [11] K.S. Coley, J. Min. Metall. B 49 (2013) 191–199.

- [12] L.Z. Yang, Z.S. Yang, G.S. Wei, Y.F. Guo, F. Chen, F.Q. Zheng, *ISIJ Int.* 59 (2019) 2272–2282.
- [13] W.J. Wang, H.X. Zhao, Y.F. Pan, B.M. Wang, K. Hou, Z.F. Yuang, *J. Iron Steel Res.* 22 (2010) No. 5, 7–10, 22.
- [14] J.G. Li, Y.N. Zeng, J.Q. Wang, Z.J. Han, *J. Iron Steel Res. Int.* 18 (2011) No. 4, 11–18.
- [15] M. Lv, R. Zhu, *Metall. Res. Technol.* 116 (2019) 502.
- [16] L. Zhong, Y. Zhu, M. Jiang, Z. Qu, Y. Za, X. Bao, *Steel Res. Int.* 76 (2005) 611–615.
- [17] M. Lv, R. Zhu, H. Wang, R. Bai, *Steel Res. Int.* 84 (2013) 304–312.
- [18] F. Liu, D. Sun, R. Zhu, F. Zhao, J. Ke, *Ironmak. Steelmak.* 44 (2017) 640–648.
- [19] F. Liu, D. Sun, R. Zhu, Y. Li, *Metall. Mater. Trans. B* 50 (2019) 2362–2376.
- [20] Q.R. Fan, in: T. Yang, W. Wang (Eds.), *International Congress on the Science and Technology of Ironmaking*, The Chinese Society for Metals, Beijing, China, 2009, pp. 1270–1274.
- [21] M.C. Díaz, S.V. Komarov, M. Sano, *ISIJ Int.* 37 (1997) 1–8.
- [22] S.L. de Souza Costa, E.P.M. de Araujo, I.L. Alves, J.L. de Siqueira, *Rev. Met. Paris* 103 (2006) 531–536.
- [23] Q.R. Fan, J.Q. Zeng, in: L.J. Jiang, J. Diao, X.S. Li, G.Q. Fan, X. Liu, T. Zhang (Eds.), *International Congress on the Science and Technology of Steelmaking*, The Chinese Society for Metals, Beijing, China, 2015, pp. 120–123.
- [24] X.B. Zhou, M. Ersson, L.C. Zhong, P.G. Jönsson, *Steel Res. Int.* 86 (2015) 1328–1338.
- [25] W.Y. Yang, C. Feng, M.L. Wang, Y.H. Lv, Y.B. Hu, X.Y. Peng, *J. Iron Steel Res.* 29 (2017) 807–815.
- [26] W. Wu, L.B. Yang, C.J. Zheng, L. Liu, *J. Iron Steel Res. Int.* 17 (2010) No. 9, 7–13.
- [27] T. Kohtani, *Steelmaking Process* 65 (1982) 211–220.
- [28] H.S. Zhang, Z.Q. Xiao, *Iron and Steel* 22 (1987) No. 9, 21–25.
- [29] S.H. Kim, R.J. Fruehan, *Metall. Trans. B* 18 (1987) 381–390.